

MPI-PhT/95-36  
 LMU-08/95  
 hep-ph/9505298  
 May 1995

# Production of $B_c$ Mesons in Hadronic Collisions<sup>1</sup>

Karol Kołodziej<sup>a,2</sup>, Arnd Leike<sup>a</sup> and Reinhold Rückl<sup>a,b</sup>

<sup>a</sup>*Sektion Physik der Universität München,  
 Theresienstr. 37, D-80333 München, FRG*

<sup>b</sup>*Max-Planck-Institut für Physik, Werner-Heisenberg-Institut,  
 Föhringer Ring 6, D-80805 München, FRG*

## Abstract

We investigate hadroproduction of  $B_c$  mesons from initial gluons using QCD perturbation theory and nonrelativistic bound state approximations. Our results obtained by two completely independent calculations are confronted with existing results which contradict each other. Moreover, we examine the approximation based on heavy quark fragmentation and determine the range of validity of it. Predictions for cross sections and differential distributions at Tevatron and LHC energies are presented.

---

<sup>1</sup>Supported by the German Federal Ministry for Research and Technology under contract No. 05 6MU93P.

<sup>2</sup> On leave from the Institute of Physics, University of Silesia, PL-40007 Katowice, Poland

# 1 Introduction

With the discovery of the top quark, it has become rather certain that  $B_c$  mesons are the only flavored heavy quark resonances which exist in nature. Although they have not yet been observed experimentally, the production rates at the Tevatron may be sizeable enough to allow for experimental identification of these interesting bound states. Clear evidence can be expected from the LHC [1], where it should also be possible to measure specific production and decay properties. This will provide valuable tests of important aspects of strong and weak interactions.

Because of the promising prospects,  $B_c$  – physics is attracting increasing attention. In particular, the hadronic production of  $B_c$  mesons has been studied by several groups [2]–[6] in the framework of QCD perturbation theory treating the  $B_c$  couplings and wave functions in a nonrelativistic approximation. There is general agreement that in  $pp$  and  $p\bar{p}$  collisions at high energies the gluon-gluon scattering process  $gg \rightarrow B_c b\bar{c}$  including higher order corrections is by far the dominant source of  $B_c$  mesons. However, the quantitative predictions derived first in refs. [2, 3, 4] in lowest order contradict each other in various respects. It is not always easy to compare the results, because of the use of different, sometimes outdated gluon momentum distributions and the lack of clear statements on the choice of scales and bound state parameters. Yet, one can convince oneself that differences in the numerical input alone cannot explain the discrepancies. The problem is most obvious in refs. [2] and [4] which disagree already on the level of the subprocess. The confusion has also not been resolved in ref. [6] which appeared very recently while we were writing up this paper. The situation is rather unsatisfactory and needs clarification.

Another controversial issue is the description of  $B_c$  hadroproduction in terms of  $b$ -pair production in  $gg$ –fusion followed by fragmentation of the  $\bar{b}$ -quark:  $gg \rightarrow b\bar{b}$ ,  $\bar{b} \rightarrow B_c b\bar{c}$ . The application of this approximation [5] was motivated by the success of the analogous approach to  $B_c$  production in  $e^+e^-$  annihilation. In fact, from the perturbative calculation of  $e^+e^- \rightarrow B_c b\bar{c}$  [7] one can directly extract the relevant fragmentation function  $D_{\bar{b}}(z)$ ,  $z$  being the momentum fraction of the  $\bar{b}$ -quark transferred to the  $B_c$  meson [8, 9]. In hadronic processes, the hard scattering formalism involving convolutions of parton cross sections with structure and fragmentation functions is generally expected to work for high- $p_T$  production. On the other hand, it has been shown in refs. [10, 11] that the fragmentation picture is not adequate for  $B_c$  production in photon-photon scattering, not even at large  $\gamma\gamma$  energies and the highest  $B_c$  transverse momenta. Since the two processes  $\gamma\gamma \rightarrow B_c b\bar{c}$  and  $gg \rightarrow B_c b\bar{c}$  are very similar at least if one disregards the gluon self–interactions and the color factors, one may mistrust the general expectation expressed above. While the previous investigations of this issue in refs. [2] and [4] are not conclusive because of the discrepancies of these calculations, ref. [12] which also appeared just recently claims the failure of the fragmentation approximation. We will clarify this important question and show that the fragmentation description indeed works to the expected accuracy.

In order to achieve these goals, we have performed two independent calculations of the dominant subprocess  $gg \rightarrow B_c b\bar{c}$  in  $O(\alpha_s^4)$  and in the usual nonrelativistic approximation. The result is compared numerically with the previous calculations. Where a comparison at the level of the subprocess was not possible, we have checked the convoluted cross sections for

the same parton distributions and input parameters as used in the calculation under examination. For the integrated cross sections, we get partial agreement with ref. [4], however for a different value of  $m_b$  and only after including a factor 1/3. Although this missing factor has been corrected in ref. [12], there are still discrepancies, in particular, in  $p_T$ -distributions. Furthermore, we clearly disagree with refs. [2, 3, 6].

For predictions on  $B_c$  production at the Tevatron and LHC the  $gg$  cross section is folded with the updated gluon distribution of ref. [13] in which the HERA measurements are taken into account. Moreover, we study in detail the dependence on the scale chosen for  $\alpha_s$  and the structure functions. Finally, we present distributions in transverse momentum and rapidity, as well as integrated cross sections including  $p_T$ - and  $y$ -cuts.

The paper is organized as follows. In chapter 2 we give details of the calculation of the matrix element and the phase space integration. There, we also specify the nominal values of all relevant parameters used in our numerical studies. Chapter 3 is devoted to total cross sections, and chapter 4 to differential distributions. A short summary and conclusions are given in chapter 5.

## 2 Calculation of the subprocess $gg \rightarrow B_c^{(*)} b\bar{c}$

To order  $\alpha_s^4$ , the subprocess  $gg \rightarrow B_c^{(*)} b\bar{c}$  is described by 36 Feynman diagrams. For the heavy  $b$  and  $c$  quarks, it is reasonable to neglect the relative momentum of the quark constituents and their binding energy relative to their masses. In this nonrelativistic limit, the constituents are on mass shell and move together with equal velocity. This implies the following relations for the masses and momenta of the  $c$ -quark,  $\bar{b}$ -quark, and the  $B_c^{(*)}$  bound state:

$$M(B_c) = M(B_c^*) = M = m_c + m_b, \quad p_c = \frac{m_c}{M}p, \quad p_{\bar{b}} = \frac{m_b}{M}p. \quad (1)$$

Furthermore, the amplitudes for the production of  $S$ -wave states are obtained from the hard scattering amplitudes for  $gg \rightarrow b\bar{b}c\bar{c}$  by applying the projection operator [14, 11]

$$v(p_{\bar{b}})\bar{u}(p_c) = \frac{f_{B_c^{(*)}}}{\sqrt{48}}(p' - M)\Pi_{SS_Z}, \quad (2)$$

where  $v(p_{\bar{b}})$  and  $\bar{u}(p_c)$  denote the respective quark spinors and  $\Pi_{SS_Z}$  is a spin projector. For a pseudoscalar state one has  $\Pi_{00} = \gamma_5$ , while for a vector,  $\Pi_{1S_Z} = \not{p}$ . From now on, we differentiate between the pseudoscalar ground state  $B_c$  and the vector ground state  $B_c^*$ . The decay constants  $f_{B_c^{(*)}}$  appearing in eq. (2) are defined by the matrix elements

$$\langle 0|\bar{b}\gamma_\mu\gamma_5 c|B_c(p)\rangle = if_{B_c}p_\mu, \quad \langle 0|\bar{b}\gamma_\mu c|B_c^*(p)\rangle = Mf_{B_c^*}\epsilon_\mu, \quad (3)$$

and are related to the bound state wave function at the origin by

$$f_{B_c} = f_{B_c^*} = \sqrt{\frac{12}{M}}|\Psi(0)|. \quad (4)$$

As in ref. [11], the color structure is not accounted for in eq. (2). The color factors are computed separately when squaring the amplitude.

In order to have an internal cross-check, we have calculated the matrix element squared by two independent methods. One calculation is based on the usual trace technique, while the other calculation makes use of helicity amplitudes similarly as in ref. [11]. The latter method is a generalization of the technique described in detail in ref. [15] for bosonic final states in  $e^+e^-$  scattering. The results of these two calculations are compared numerically for different sets of particle momenta and found to agree to seven digits. Furthermore, it has been checked that the matrix element vanishes when the polarization vector of anyone of the initial gluons is substituted by the momentum vector of this gluon.

The phase space integration is also performed independently using two different routines. In a first step, the integration routines are checked for the pure 3-particle phase space and found to agree numerically with the corresponding analytical formulae to four digits for all distributions considered. Before integrating the matrix element squared with the help of the Monte Carlo routine **VEGAS** [16], the strongest peaks of it were smoothed out by introducing new integration variables. After the integration all differential distributions and cross sections of the two independent calculations agree within the Monte Carlo errors.

In addition, we have calculated cross sections and distributions for  $b\bar{b}(c\bar{c})$  production and subsequent fragmentation of the  $\bar{b}(c)$ -quark, that is for  $gg \rightarrow b\bar{b}$ ,  $\bar{b} \rightarrow B_c\bar{c}$  and  $gg \rightarrow c\bar{c}$ ,  $c \rightarrow B_c b$ , respectively. The relevant fragmentation functions  $D_{\bar{b}}(z)$  and  $D_c(z)$  are known from perturbation theory [8]. In  $e^+e^- \rightarrow B_c\bar{c}b$ , they provide a perfect approximation for the energy distribution  $d\sigma/dz$  with an error of the order of  $M^2/s$ ,  $\sqrt{s}$  being the c.m. energy [8, 9]. In contrast, in  $\gamma\gamma \rightarrow B_c\bar{c}b$  above threshold, the fragmentation mechanisms are dominated by quark recombination processes. This can be shown in a gauge invariant way without actually factorizing the process in heavy quark production and fragmentation [11]. Because of the similarity of the underlying processes, one anticipates recombination dominance in  $gg \rightarrow B_c\bar{c}b$  at least at low  $p_T$ . Concerning the fragmentation mechanism, we stress that the factorized description  $d\hat{\sigma}(gg \rightarrow b\bar{b}) \otimes D_{\bar{b}}(z)$  is not justified at small  $p_T$  and close to threshold, where the quark masses are important. This caveat is ignored in ref. [12]. In order to find out where and to what extent this approximation can be trusted, we have also assumed various relations between daughter and parent momenta:

$$p_T = z\sqrt{\hat{s}/4 - \mu^2} \sin \theta_b, \quad p_L = p_T \cot \theta_b, \quad \mu = M \text{ (I)}, \quad m_b \text{ (II)}, \quad 0 \text{ (III)}, \quad (5)$$

where  $\sqrt{\hat{s}}$  is the gluon-gluon c.m. energy. The case I respects the physical phase space boundaries, II and III are assumed in refs. [5] and [12], respectively. These prescriptions are equivalent to the accuracy of the fragmentation approach.

To obtain cross sections for  $pp$  or  $p\bar{p}$  collisions, the gluon-gluon cross section  $\hat{\sigma}$  has to be folded with the gluon structure functions  $g(x, Q^2)$  of the (anti)proton:

$$\sigma(s) = \int_0^1 dx_1 \int_0^1 dx_2 g(x_1, Q^2) g(x_2, Q^2) \theta(x_1 x_2 s - 4M^2) \hat{\sigma}(s x_1 x_2, Q^2). \quad (6)$$

Analogous convolution formulae hold for differential distributions. For numerical illustrations we use the following input

$$f_{B_c} = f_{B_c^*} = 0.4 \text{ GeV}, \quad m_b = 4.8 \text{ GeV}, \quad m_c = 1.5 \text{ GeV} \quad (7)$$

together with the MRS(A') gluon distribution [13]. The strong coupling constant  $\alpha_s(Q^2)$  entering  $\hat{\sigma}$ , is taken in leading logarithmic approximation:

$$\alpha_s(Q^2) = \frac{\alpha_s(m_Z^2)}{1 + \frac{33-2n_f}{12\pi} \alpha_s(m_Z^2) \ln(\frac{Q^2}{m_Z^2})} \quad (8)$$

with  $n_f = 5$  and  $\alpha_s(m_Z^2) = 0.113$ . This is the normalization of the running coupling in the MRS(A') parton distributions. As is usually done in such calculations, we identify the scale of  $\alpha_s$  with the evolution scale of the structure functions.

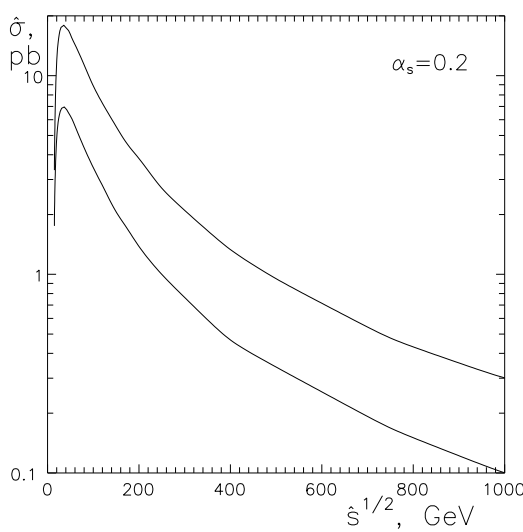


**Fig. 1.** Integrated cross sections for  $gg \rightarrow B_c^{(*)} b\bar{c}$  versus the c.m. energy. The lower (upper) curve corresponds to  $B_c$  ( $B_c^*$ ) production.

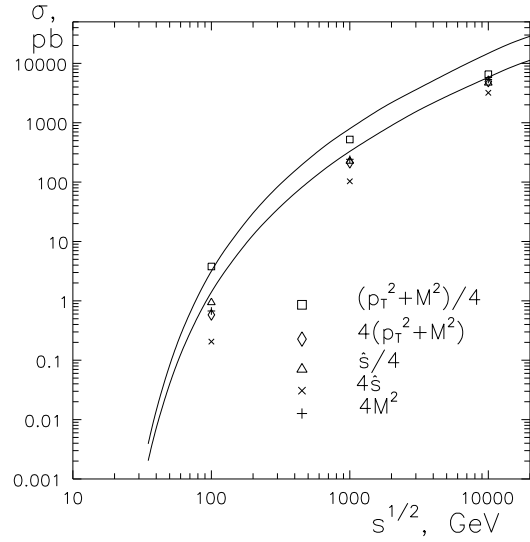


**Fig. 2.** Total cross sections for  $pp(p\bar{p}) \rightarrow B_c^{(*)} b\bar{c} + X$  versus the c.m. energy. The lower (upper) curve corresponds to  $B_c$  ( $B_c^*$ ) production calculated with the scale  $Q^2 = p_T^2 + M^2$ . The symbols refer to other choices.

### 3 Total cross sections

First we present the parton cross sections  $\hat{\sigma}(\hat{s})$  for the subprocess  $gg \rightarrow B_c^{(*)} b\bar{c}$ , and the convoluted production cross sections for  $pp$  and  $p\bar{p}$  to  $B_c^{(*)} b\bar{c} + X$ . Then we confront our results with results in the published and unpublished literature [2, 3, 4, 6].

Figures 1 and 2 illustrate our main findings. The partonic cross sections are shown in Fig. 1 for a fixed value of  $\alpha_s$  in order to facilitate comparison with other calculations. The production threshold is located at  $\sqrt{\hat{s}} = 2(m_b + m_c) = 12.6$  GeV. At sufficiently high energies, the cross sections fall roughly like  $1/\hat{s}$ . Moreover, the  $B_c^*$  cross section is approximately three times as large as the  $B_c$  cross section as expected from spin counting.

The total hadronic cross sections for  $B_c$  and  $B_c^*$  production are plotted in Fig. 2. One can see the typical rise of  $\sigma$  with energy reflecting the rise of the gluon density as  $x$  approaches

|                              | 20 GeV  | 40 GeV  | 100 GeV | 1 TeV    |
|------------------------------|---------|---------|---------|----------|
| $\hat{\sigma}_{B_c}$         | 8.27(2) | 12.7(1) | 6.67(4) | 0.208(2) |
| $\hat{\sigma}_{B_c}$ , [4]   | 29.3(1) | 40(1)   | 21(1)   | 0.27(4)  |
| $\hat{\sigma}_{B_c^*}$       | 20.3(1) | 33.1(2) | 17.4(1) | 0.61(1)  |
| $\hat{\sigma}_{B_c^*}$ , [4] | 71.6(3) | 105(2)  | 56(2)   | 0.6(1)   |

Table 1: Comparison of total cross sections in pb for  $gg \rightarrow B_c^{(*)} b\bar{c}$  with the corresponding results of ref. [4]. The input parameters are  $m_b = 5.1$  GeV,  $m_c = 1.5$  GeV,  $\alpha_s = 0.2$  and  $f_{B_c} = f_{B_c^*} = 0.57$  GeV. The number in parenthesis shows the Monte Carlo uncertainty in the last digit.

$x_{min} = 4(m_b + m_c)^2/s$ , and the peaking of  $\hat{\sigma}$  near threshold. A similar behaviour is observed for  $B_c^{(*)}$  production in the scattering of two bremsstrahlung photons radiated from  $e^\pm$ -beams [11]. The scale dependence is also exhibited in Fig. 2 for a variety of choices including the fixed scale  $Q^2 = 4M^2$ . At relatively low energies, the predictions vary by more than one order of magnitude. At higher energies, however, the results become more stable changing only within a factor two. It is interesting to note in this respect that the differences resulting from convolution with the gluon densities MRS(A') of ref. [13] and CTEQ2 of ref. [17] are very small. In fact, they would be invisible in Fig. 2. In addition to the scale uncertainty which can only be reduced by calculating the next-to-leading corrections, a formidable task indeed, one has uncertainties connected with the decay constants  $f_{B_c^{(*)}}$  and the effective quark masses  $m_b$  and  $m_c$ . These amount at least to another factor of two.

Next, we confront our results with the numerical results of refs. [2, 3, 4, 6]. The comparison is easiest and clearest for the parton cross section  $\hat{\sigma}$ , where one does not have to pay attention to different parametrizations of the gluon distribution and for a constant value of  $\alpha_s$ . Needless to say, we have always adopted the same values for  $m_b$ ,  $m_c$  and  $f_{B_c^{(*)}}$  as the reference calculation.

Table 1 summarizes the comparison with ref. [4]. As can be seen, we clearly disagree with this calculation. Amazingly, if one uses instead of the quark masses quoted the masses given in eq. (7) one achieves agreement at  $\sqrt{s} = 20, 40$  and  $100$  GeV within the Monte Carlo errors, up to a color factor  $1/3$  which has apparently been missed. In the recent repetition [12] of their calculation, the authors account for the missing color factor. However, we do not see an explanation for the remaining discrepancy at  $\sqrt{s} = 1$  TeV which exceeds the MC uncertainty by far. We also observe a clear discrepancy with ref. [6] as demonstrated in Table 2. The fact that these authors claim rough agreement with ref. [4] speaks against their results because of the error in the color factor pointed out above.

Furthermore, results on the  $gg$ -cross section can be found in the second paper of ref. [2]. Unfortunately, since the choice of the QCD-scale  $\Lambda$  and of the momentum scale  $Q^2$  is left unclear, a direct comparison is difficult. In Table 3, we try two hypotheses: fixed  $\alpha_s$  and  $\alpha_s(\epsilon\hat{s})$ , where the numerical factor  $\epsilon$  can be chosen arbitrarily. As one can see, in none of the two cases we are able to achieve agreement.

Finally, the hadronic cross sections given in ref. [3] seem to differ even by more than one order

|                            | 20 GeV  | 30 GeV  | 40 GeV  | 60 GeV  | 80 GeV  | 100 GeV |
|----------------------------|---------|---------|---------|---------|---------|---------|
| $\hat{\sigma}_{B_c}$       | 6.86(2) | 9.71(4) | 9.74(5) | 7.93(5) | 6.23(5) | 5.01(4) |
| $\hat{\sigma}_{B_c}$ , [6] | 23.6    | 26.0    | 22.3    | 15.5    | 11.2    | 8.4     |

Table 2: Comparison of the total cross section in pb for  $gg \rightarrow B_c b\bar{c}$  with the result of ref. [6]. The input parameters are  $m_b + m_c = 6.3$  GeV,  $m_b = 3m_c$ ,  $\alpha_s = 0.2$  and  $f_{B_c} = 0.50$  GeV. The number in parenthesis shows the Monte Carlo uncertainty of the last digit.

| $\sqrt{\hat{s}}$ [GeV] | Ref. [2] | fixed $\alpha_s$ | $\alpha_s(\epsilon\hat{s})$ |
|------------------------|----------|------------------|-----------------------------|
| 20                     | 4.9      | 4.9              | 4.9                         |
| 30                     | 8.5      | 7.0              | 5.0                         |
| 60                     | 7.9      | 5.9              | 2.4                         |

Table 3: Comparison of the total cross section  $\hat{\sigma}(gg \rightarrow B_c b\bar{c})$  (in pb) for fixed and running  $\alpha_s$  with the result quoted in ref. [2]. The input parameters are  $m_b = 4.9$  GeV,  $m_c = 1.5$  GeV, and  $f_{B_c} = 0.48$  GeV. The normalization of  $\alpha_s$  is chosen such as to reproduce the cross section at 20 GeV.

of magnitude from our results. Again, since the normalization of  $\alpha_s(Q^2)$  is not specified, we cannot make a more definite statement.

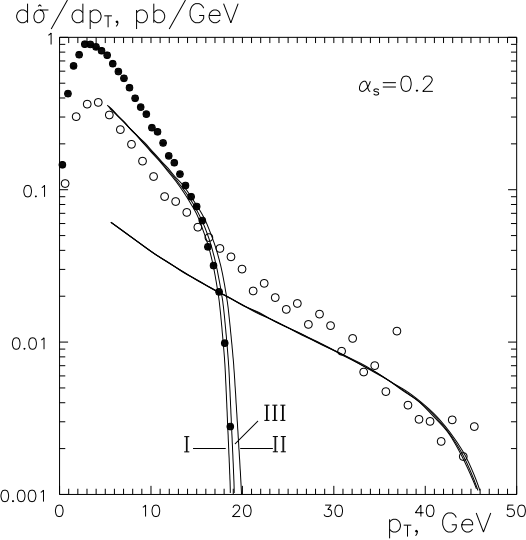
To conclude, all previous calculations [2, 3, 4, 6] are in mutual disagreement. Our calculation confirms the results on  $\hat{\sigma}$  of ref. [4] at  $\sqrt{\hat{s}} \leq 100$  GeV when including the missing color factor [12] and taking  $m_b = 4.8$  GeV. However, at  $\sqrt{\hat{s}} = 1$  TeV, a clear numerical discrepancy remains.

## 4 Distributions

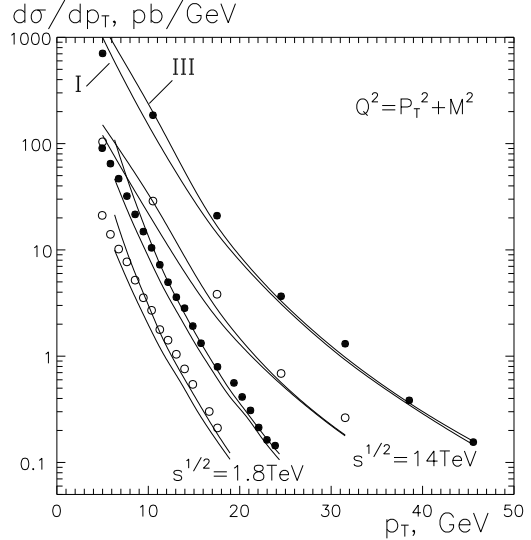
Having discussed the total  $B_c^{(*)}$  production cross sections, we now turn to the differential distributions in transverse momentum and rapidity. Since they are very similar for  $B_c$  and  $B_c^*$ , we show them for the pseudoscalar meson only. Moreover, since the sensitivity to the scale in  $\alpha_s(Q^2)$  and  $g(x, Q^2)$  is already indicated in Fig. 2, we shall present here results only for the scale  $Q^2 = p_T^2 + M^2$ . Finally, we will examine the fragmentation description and determine the region of validity of this approximation. In order to be consistent with the complete calculation at the fixed order  $\alpha_s^4$ , we do not take into account evolution effects in the fragmentation function  $D_b(z)$ . These effects are studied in ref. [5]. Moreover, it should be mentioned that  $c$ -quark production and fragmentation is negligible.

Fig. 3 illustrates the main features of the subprocess  $gg \rightarrow B_c b\bar{c}$ . We see that the fragmentation description approaches the  $p_T$ -distributions resulting from the complete calculation only in the tails of the distributions. At  $\sqrt{\hat{s}} \leq 40$  GeV a problem arises also when  $p_T$  approaches  $p_T^{max}$  because of mass ambiguities in the phase space boundaries of the fragmentation approach.

These effects increase as  $\hat{s}$  decreases and are largest for the prescription III of eq. (5). On the other hand, if the physical phase space boundary is imposed on the fragmentation approach as in eq. (5) case I, the approximation slightly improves. Comparing Fig. 3 with Fig. 5 of ref. [11], one sees that in contrast to  $\gamma\gamma \rightarrow B_c b\bar{c}$  where heavy quark fragmentation is completely subdominant even at large  $p_T$ , in  $gg \rightarrow B_c b\bar{c}$  it provides a good approximation at large  $\hat{s}$  and  $p_T$ . Obviously, the presence of gluon self-couplings and color factors has a drastic influence on the relative importance of the fragmentation and recombination.



**Fig. 3.** Transverse momentum distributions of the  $B_c$  in  $gg \rightarrow B_c b\bar{c}$  at  $\sqrt{\hat{s}} = 40$  and  $100$  GeV: complete  $O(\alpha_s^4)$  calculation (circles) and fragmentation approximation (solid curves). The labels I–III refer to the kinematics specified in eq. (5).



**Fig. 4.** Transverse momentum distribution of the  $B_c$  at Tevatron and LHC energies: complete  $O(\alpha_s^4)$  calculation (circles) and fragmentation approximation (solid curves). The labels I and III refer to the kinematics specified in eq. (5). At each energy, results are shown without a rapidity cut (full circles) and for  $|y| \leq 0.5$  (empty circles).

Distributions in  $p_T$  for  $pp$  (and  $p\bar{p}$ ) collisions are displayed in Fig. 4. Also shown is the effect of a stringent cut in rapidity. A few comments are in order. Most importantly, after convolution the full calculation and the fragmentation description are in reasonable agreement at  $p_T \geq 10$  GeV. This can be understood from the properties of the unfolded  $p_T$ –distributions illustrated in Fig. 3 and from the rise of the gluon density at small  $x$  which favours contributions from the smallest possible subenergies  $\hat{s}$ . At  $p_T < 10$  GeV, the deviation grows indicating that one is getting outside the range of validity of the fragmentation picture. Furthermore, the sensitivity to the kinematical prescription, eq. (5), decreases slowly with increasing  $p_T$ . Beyond the  $p_T$ –region considered in Fig. 4, it can be safely ignored. These observations are rather independent of the rapidity cut. The rapidity distributions exhibit the usual plateau region around  $y = 0$ , as shown in Fig. 5.

Thus, in contradiction to ref. [12], we find that the fragmentation description provides a good approximation for  $p_T \geq 10$  GeV. The deviation from the complete  $O(\alpha_s^4)$  results is much

smaller than the uncertainties in the scale  $Q^2$ , in the decay constant  $f_{B_c^{(*)}}$ , and in the effective values of  $m_b$  and  $m_c$ .

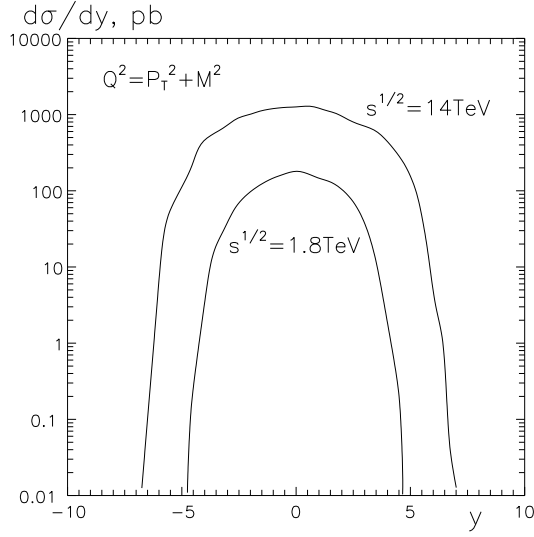


**Fig. 5.** The rapidity distributions of the  $B_c$  mesons at Tevatron and LHC energies.

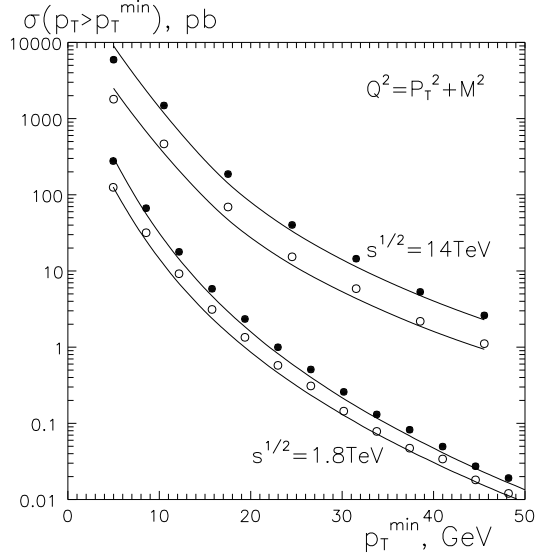


**Fig. 6.** Integrated production cross sections for the  $B_c$  as functions of the minimum  $p_T$  cut: complete  $O(\alpha_s^4)$  calculation (circles) and fragmentation approximation using eq. (5) II (solid curves). For each energy, results are shown without a rapidity cut (full circles) and for  $|y| \leq 1$  (empty circles).

## 5 Summary and conclusions

We have presented new results on  $B_c$  meson production in  $pp$  and  $p\bar{p}$  collisions derived from the  $O(\alpha_s^4)$  subprocess  $gg \rightarrow B_c^{(*)}b\bar{c}$  using nonrelativistic bound state approximations. We have performed two independent calculations employing two different methods. We therefore believe that our results which deviate from all previous calculations [2, 3, 4, 6, 12] are correct.

In addition, we have determined the range of validity of the fragmentation approximation with the heavy quark fragmentation function  $D_{\bar{b}}(z)$  as calculated in perturbation theory [8]. For  $p_T \geq 10$  GeV, we find good quantitative agreement between the fragmentation description and the complete calculation. At  $p_T = 5 - 10$  GeV, mass ambiguities in the fragmentation kinematics lead to effects up to a factor of two. Below 5 GeV, the fragmentation approximation brakes down.

In order to evaluate the observability of  $B_c$  mesons at the Tevatron and LHC, it is useful to integrate the  $p_T$ -distributions of Fig. 4 over  $p_T \geq p_T^{min}$ . The resulting cross sections are plotted in Fig. 6. This estimate indicates a production of the order of  $10^4$   $B_c$  mesons with  $p_T^{min} = 10$  GeV at the Tevatron, assuming an integrated luminosity of  $100 \text{ pb}^{-1}$ . Contributions from the production and decay of  $B_c^*$  mesons and heavier states are not yet taken into account in this number (see e.g. ref. [5]). This rate may be sufficient for a first observation in the

decay channels  $B_c \rightarrow J/\psi X$ , for which a branching ratio of the order of 10% is predicted [18]. Finally, at the LHC for  $100\text{fb}^{-1}$  one can expect  $10^7$  direct  $B_c$  mesons at  $p_T^{\min} = 20\text{ GeV}$  which should make  $B_c$  physics a very interesting topic.

## References

- [1] ATLAS Collab., Technical Proposal, CERN/LHCC/94-43; E. Albio et al., Altlas Internal Note PHYS-NO-058.
- [2] C.-H. Chang, Y.-Q. Chen, Phys. Rev. **D48** (1993) 4086; C.-H. Chang, Y.-Q. Chen, G.-P. Han, H.-T. Jiang, AS-ITP-94-24, hep-ph/9408242.
- [3] S.R. Slabospitsky, IHEP 94-53, hep-th/9404346.
- [4] A.V. Berezhnoy, A.K. Likhoded, M.V. Shevlyagin, IHEP 94-48, hep-ph/9408284.
- [5] K. Cheung, Phys. Rev. Lett. **71** (1993) 3413; K. Cheung, T.C. Yuan, UCD-95-4, CPP-94-37, hep-ph/9502250.
- [6] M. Masetti, F. Sartogo, hep-ph/9503491.
- [7] L. Clavelli, Phys. Rev. **D26** (1982) 1610; C.-R. Ji, R. Amiri, Phys. Rev. **D35** (1987) 3318; V. Barger, K. Cheung, W.-Y. Keung, Phys. Rev. **D41** (1990) 1541; C.-H. Chang, Y.-Q. Chen, Phys. Lett. **B284** (1992) 127.
- [8] F. Amiri, C.-R. Ji, Phys. Lett. **B195** (1987) 593; C.-H. Chang, Y.-Q. Chen, Phys. Rev. **D46** (1992) 3845; E. Braaten, K. Cheung, T.C. Yuan, Phys. Rev. **D48** (1993) R5049.
- [9] A. Leike, R. Rückl, Nucl. Phys. **B** (Proc. Suppl.) **37B** (1994) 215.
- [10] A.V. Berezhnoy, A.K. Likhoded, M.V. Shevlyagin, hep-ph/9408287, Phys. Lett. **B342** (1995) 351.
- [11] K. Kołodziej, A. Leike, R. Rückl, MPI-PhT/94-84, LMU-23/94, hep-ph/9408287, to appear in Phys. Lett. **B**.
- [12] A.V. Berezhnoy, A.K. Likhoded, O.P. Yushchenko, IHEP-95-59, hep-ph/9504302.
- [13] A.D. Martin, W.J. Stirling, R.G. Roberts, RAL-95-021, DTP/95/14, hep-ph/9502336.
- [14] B. Guberina, J.H. Kühn, R.D. Peccei, R. Rückl, Nucl. Phys. **B174** (1980) 317.
- [15] K. Kołodziej, M. Zrałek, Phys. Rev. **D43** (1991) 3619.
- [16] G.P. Lepage, J. Comp. Phys. **27** (1978) 192.
- [17] H.L. Lai, Michigan preprint MSU-HEP-41024, hep-ph/9410404.
- [18] D. Du, Z. Wang, Phys. Rev. **D39** (1989) 1342; M. Lusignoli, M. Masetti, Z. Phys. **C51** (1991) 549; V.V. Kiselev, A.K. Likhoded, A.V. Tkabladze, Phys. At. Nucl. **56** (1993) 643; Likhoded et al., Nucl. Instrum. Methods **A333** (1993) 209; P. Colangelo, G. Nardulli, N. Paver, Z. Phys. **C57** (1993) 43.